A New, Rapid, Colorimetric Chemodosimeter, 4(pyrrol-1-Yl)pyridine, for Nitrite Detection in Aqueous Solution

Mallory E. Thomas , Lynn D. Schmitt , Alistair J. Lees *

Posted Date: 6 December 2023

doi: 10.20944/preprints202312.0412.v1

Keywords: aggregate; chemodosimeter; limit of detection; nitrite

Article

A New, Rapid, Colorimetric Chemodosimeter, 4(Pyrrol-1-yl)pyridine, for Nitrite Detection in Aqueous Solution

Mallory E. Thomas [1], Lynn D. Schmitt [2] and Alistair J. Lees [1,*]

[1] Department of Chemistry, Binghamton University, Binghamton, NY
[2] Department of Chemistry, SUNY Cortland, Cortland, NY
* Correspondence: alees@binghamton.edu

Abstract: With increasing concerns over environmental impact, and overall health of both the environment and its people, a need to quantify contaminants is of the utmost importance. Chemosensors with low detection limits and relative ease of application can address this challenge. Nitrite ions are known to be detrimental to both the environment and human health. A new colorimetric chemodosimeter has been prepared from a homolytic photochemical cleavage of a reaction between pyrrole and pyridine. The product, 4(pyrrol1-yl)pyridine, yields a limit of detection of 0.330 (±0.09) ppm for the detection of nitrite in aqueous solution, employing a colorimetric change from yellow to pink. It is also highly selective for nitrite when various competitive anions such as SO_3^{2-}, NO_3^-, PO_4^{3-}, SO_4^{-2}, Cl^-, F^-, I^-, Br^-, and CN^- are present in great excess. The molecule's especially high sensitivity to nitrite is apparently the result of a complex supramolecular mechanism, characterized by both dynamic light scattering of the aggregate and the Tyndall effect. Consequently, this new sensor provides a simple, low-cost way to rapidly detect nitrite anions in aqueous solution.

Keywords: aggregate; chemodosimeter; limit of detection; nitrite

1. Introduction

As key components of the nitrogen cycle, nitrate and nitrite are commonly found infiltrated into both surface and ground water systems. This is primarily due to contamination by animal waste, fertilizer, or as a result of agricultural runoff [1–5]. The maximum contaminant level (MCL) of nitrite set by the U.S Environmental Protection Agency (EPA) is 1 ppm [1]. Its high water solubility, in tandem with the low retention capability by soil, makes entryway in water systems easier [6]. However, their heightened ubiquity in water systems contributes to detrimental effects to aquatic ecosystems. Their environmental impact is attributed to anthropogenic nutrient pollution which ultimately leads to eutrophication and can prove disastrous for aquatic ecosystems [7–10]. Additionally, the increased usage of nitrite in other capacities such as additives in the food industry, preservative science, and agricultural means has resulted in overall elevated nitrite concentrations [5,11,12].

Trace amounts of nitrites pose a risk to human health. They are considered type A inorganic chemicals, which require detailed monitoring due to their potential risks [13,14]. The World Health Organization (WHO) has enforced a limit of 3 ppm of nitrite in drinking water [5]. Typically, nitrite is found in consumer goods such as beets, lettuce, and meat. Once combined with salt, it is thought to be the curing component that preserves food and provides the iconic pinkish colour and fresh flavour of meat products [15–19]. While nitrites are primarily obtained through a diet of vegetables and cured meat, small amounts are also found in fish and dairy products. Here, meat products typically contain <0.2-6.4 mg of nitrite per kilogram, while dairy products contain <0.2-1.7 mg of nitrite per kilogram [5]. The presence of nitrite in consumer goods serves to prevent the growth of bacteria that can cause botulism disease [20,21]. However, its use as preservative has been shown to

 doi:10.20944/preprints202312.0412.v1

have a probable connection between colorectal and stomach cancers in those with a high intake of cured meat [22]. Even these aforementioned trace amounts of nitrite ions are hazardous to human health. Nitrite contaminated water has even caused shortness of breath and blue baby syndrome in infants once digested [1,3,14]. In the body, nitrite can interact with haemoglobin to form methaemoglobin where iron is oxidized to Fe^{3+}. Here, haemoglobin loses the ability to carry and release oxygen throughout the body and can cause hypoxia most notably to the central nervous system [5,23,24]. Nitrite also plays a key role in human physiology as a signalling component [25]. However, after interacting with proteins, nitrites play a role in the generation of carcinogenic N-nitrosamines [26] which can lead to gastric cancer [27–30]. Common symptoms can range from cardiac dysrhythmias, mild dizziness, lethargy, and be as dire as a coma or convulsions [31]. It is also suggested that it is an indicator of bacterial contamination [32]. In addition, elevated risk of non-Hodgkin's lymphoma has been reported [33]. It has previously been reported that concentrations ranging from 33-250 mg of nitrite per kg of body weight is lethal, with 0.4-200 mg/kg of body weight enough to cause methaemoglobinemia [34].

Common detection methods for nitrite employ electrochemical methods [35,36], fluorescence spectroscopy [37–40], UV-visible spectroscopy [39], chemiluminescence [41,42], chromatography, and flow injection analysis [43]. However, many of these methods are susceptible to interference from other particles in water, have high cost, need for sophisticated equipment, are exceedingly complicated with intricate experimental steps, and consume high amounts of materials. Nitrite also has the potential to be indirectly detected in colorimetric assays that employ a diazotization reaction between nitrite and sulphanilamide, but these are prone to interference from other agents [44–46]. To alleviate these challenges, there is a priority for development of sensors with increased sensitivity, selectivity, lower cost, and increased ease of portability. From this, a large variety of compounds have been employed to create nitrite sensors such as nanoparticles, metal oxides, carbon materials [36,47], and other organic frameworks [40]. However, colorimetric methods are still the most highly sought after for their portability, simplicity, and the rapid response seen with the naked eye [48,49]. Here, we offer a new colorimetric organic chemodosimeter, 4(pyrrol-1-yl)pyridine, that reveals both high sensitivity and selectivity to nitrite in aqueous solutions. Its rapid response and detection limit of 0.330 (±0.09) mg/L offers a solution to the need for low cost, portable, and efficient nitrite sensors.

2. Materials and Methods

2.1. Reagents

All materials were purchased commercially and used as received unless specified. The following materials were used; methylene chloride (Fisher, 99%), pyrrole (Fisher, 99%), 4-chloropyridine hydrochloride (Sigma, 99%), hydrochloric acid (Fisher, 98%), sodium carbonate (Fisher, 99%), anhydrous sodium sulphate (Fisher, 99%) , sodium nitrate (Fisher, 99%), sodium nitrite (Fisher, 99%) sodium phosphate (Fisher, 99%), sodium chloride (Fisher, 99%), sodium fluoride (Fisher, 99%), sodium bromide (Fisher, 99%), potassium iodide (Fisher, 99%), potassium cyanide (Fisher, 99%), dimethyl sulfoxide (Fisher, 99%), and chloroform (Fisher, 99%). Spectroscopy grade 18 MΩ water was used as solvent, unless otherwise specified.

2.2. Synthesis of 4(pyrrol-1-yl)pyridine

Synthesis of a new molecule, 4(pyrrol-1-yl)pyridine, was carried out using an analogous procedure for a related compound previously published by Seki et al [50,51]. The synthesis of 4(pyrrol-1-yl)pyridine was carried out in a 1:28 ratio of 4-chloropyridine hydrochloride (0.001 mol) to freshly distilled pyrrole (0.028 mol). In a 250-mL quartz round-bottom flask, 4-chloropyridine hydrochloride (0.150 g) was dissolved in pre-dried methylene chloride (100 mL) and allowed to stir under bubbling of nitrogen gas for one hour. The mixture was irradiated while stirring under a constant flow of nitrogen. Typically, after a few minutes, the solution begins to turn yellow, and continues to deepen colour throughout photolysis. Prolonged light exposure after twenty minutes leads to the formation of black polypyrrole side products. The reaction is monitored via UV-visible

 doi:10.20944/preprints202312.0412.v1

spectroscopy until completion. The product, 4(pyrrol-1-yl)pyridine, was extracted with three washes of 10% hydrochloric acid for a volume of 30 mL total. The aqueous layer was separated and neutralized using solid sodium bicarbonate until a neutral pH was reached, and measured via a pH probe. The neutralized aqueous layer was extracted with four washes of dried dichloromethane for a volume of 20 mL total. The resulting yellow-orange organic solution was dried via solid anhydrous sodium sulphate, decanted, and the liquid was subsequently concentrated to dryness to yield an orange oil. The resulting product was stored in 297 K to aid in its preservation.

2.3. Instrumentation and Procedures

UV-visible spectra were taken on a Shimadzu UV-vis spectrometer in spectroscopy grade 18 MΩ water, unless otherwise stated. Spectra were recorded at 303 K in a 1.00-cm path length quartz cuvette and baselines were set with 18 MΩ water as a reference, unless indicated otherwise. An Oriel Mercury/Xenon medium pressure lamp (200 W) was used for the photochemical synthesis of 4(pyrrol-1-yl)pyridine. All NMR data was recorded on a Bruker NEO 400 MHz spectrometer in 99.9% pure $CDCl_3$, 99% pure D_2O, or 99% pure D-DMSO, and high precision 535-pp NMR tubes were used. Dynamic Light Scattering (DLS) data was obtained using a Malvern Zetasizer Lab using 18 MΩ water as a solvent at room temperature in Malvern Zetasizer nano series plastic cuvettes. The volumes used matched the minimum volume of the instrument being approximately 1 mL. The refractive index used was 1.59. Five duplicates were obtained with an equilibrium time of 20 s, using a side scatter angle of detection.

2.4. Titration with 1 x 10^{-2} M sodium nitrite (aq.)

All aqueous solutions of 4(pyrrol-1-yl)pyridine were recorded immediately after dissolution in 18 MΩ water to avoid any thermal degradation. A freshly prepared solution of 4(pyrrol-1-yl)pyridine was made in 18 MΩ water and UV-visible spectra were recorded over the range of 200-800 nm. A sample of 1.00 x 10^{-2} M aqueous sodium nitrite was prepared in a 100.00 mL volumetric flask and mixed until homogeneous. Titrations of 2.00 µL (1.00 x 10^{-2} M) sodium nitrite were injected into 2.00 mL of aqueous 4(pyrrol-1-yl)pyridine via a micropipette. The subsequent spectra were monitored via UV-visible spectroscopy immediately upon addition of nitrite, and the colorimetric change from yellow to pink was also observed using the naked eye. Plots for the limit of detection determinations (LOD) used the starting absorbance at 509 nm of the sensor (A_{sensor}), absorbance upon each successive addition of nitrite at 509 nm ($A_{nitrite}$), maximum absorbance at 509 nm after all additions of nitrite (A_{max}), and the minimum absorbance at 509 nm (A_{min}). Errors for the limit of detection values were obtained from the standard deviation of ten measurements.

2.5. Competitive anion titrations

A freshly prepared solution of 4(pyrrol-1-yl)pyridine of various concentrations were made in 18 MΩ water. Competitive anion solutions were made in 1:50 ratios (1.00 x 10^{-2} M nitrite, 0.5 M competing anion) in 100 mL volumetric flasks using their sodium or potassium salts. Typically 2.26 x 10^{-3} M to 2.75 x 10^{-3} M 4(pyrrol-1-yl)pyridine solutions were titrated with 1.00 µL injections for a total of 4 additions (4.00 µL). Spectra upon each addition were monitored via UV-visible spectroscopy.

2.6. Dynamic Light Scattering

Approximately 1 mL aqueous samples of 4(pyrrol-1-yl)pyridine in 18 MΩ water were inserted into a plastic cuvette matching the required volume minimum of the instrument. Five trials were recorded per sample employing a refractive index of 1.59, equilibration time of 20 s, and a side scatter angle of detection.

Preprints (www.preprints.org) | NOT PEER-REVIEWED | Posted: 6 December 2023 doi:10.20944/preprints202312.0412.v1

2.7. Tyndall Effect

Approximately 4 mL aqueous samples of 4(pyrrol-1-yl)pyridine were irradiated with light from a helium laser in a dark room to determine if light scattering was present.

3. Results and Discussion

3.1. Synthesis and Characterization of 4(pyrrol-1-yl)pyridine

The reaction between pyrrole and pyridine, producing 4(pyrrol-1-yl)pyridine, appears to be a radical-generated photoprocess, with prolonged light exposure leading to the formation of polypyrrole. Scheme 1 illustrates the proposed two-step reaction mechanism initiated by light. The energy of irradiation due to the Hg/Xe lamp is sufficiently high in energy to homolytically cleave both the C-Cl bond of 4-chloropyridine (338.2 kJ/mol) and the N-H bond of pyrrole (351 kJ/mol) [52].

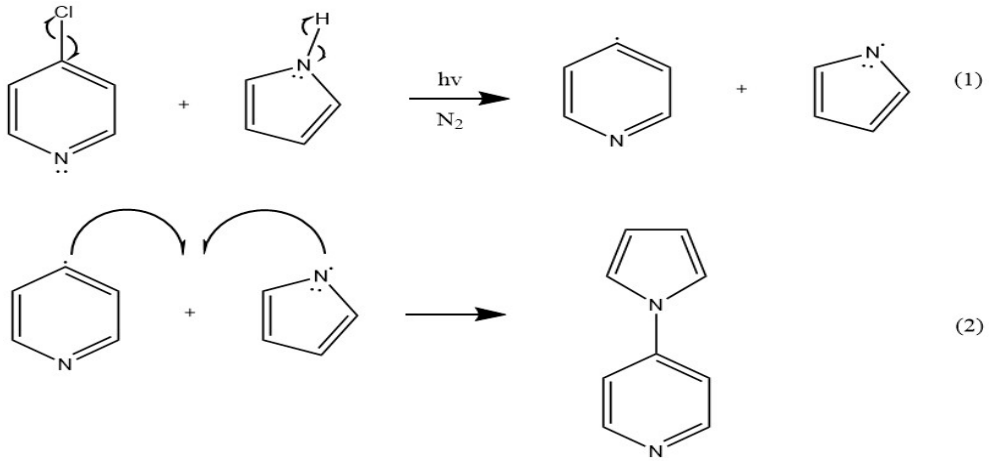

Scheme 1. Proposed two-step reaction mechanism for the synthesis of 4(pyrrol-1-yl)pyridine.

Confirmation of the resulting product 4(pyrrol-1-yl)pyridine via ^{1}H NMR in $CDCl_3$ yields δ8.44 (dd, 2H), δ7.23 (dd, 2H), δ6.73 (dd 2H) and δ6.17 (dd, 2H) with equal integrations. Additionally, ^{13}C NMR assignments further confirm the creation of 4(pyrrol-1-yl)pyridine with the following chemical shifts: δ150.75, δ144.14, δ124.22, δ117.68, and δ108.09. This was found to be consistent with previously determined NMR positions [53–55]. ^{1}H and ^{13}C NMR assignments are designated on the structure of 4(pyrrol-1-yl)pyridine in Scheme 2.

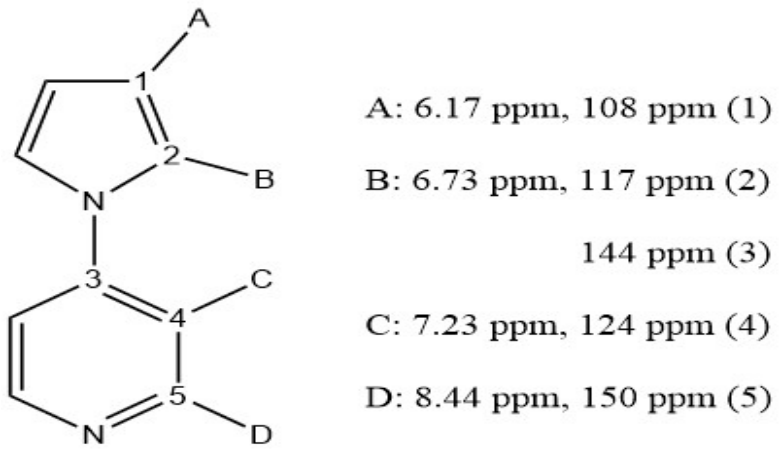

Scheme 2. 4(pyrrol-1-yl)pyridine with ^{1}H and ^{13}C NMR assignments.

Two dimensional ^{1}H NMR (COSY, HSQC) further confirm synthesis of 4(pyrrol-1-yl)pyridine by depicting H-bond interactions between the pyrrole hydrogens, and the pyridine hydrogens on the molecule, see Supporting Information. ^{1}H NMR concentration studies of 4(pyrrol-1-yl)pyridine were

Preprints (www.preprints.org) | NOT PEER-REVIEWED | Posted: 6 December 2023 doi:10.20944/preprints202312.0412.v1

carried out in $CDCl_3$ to determine any changes in structural determination. A dilute (<10% v/v) sample of 4(pyrrol-1-yl)pyridine yields sharp peaks with clear splitting, and approximately equal integrations of 1.00, 1.04, 0.72, and 0.71 However, more concentrated samples of 4(pyrrol-1-yl)pyridine of 10% (v/v) and 40% (v/v) sensor in $CDCl_3$ depicted a significant downfield shift of both pyridine protons and significant peak broadening indicative of intermolecular interactions respectively. Here, integrations were also approximately equal to one with the 10% 4(pyrrol-1-yl)pyridine spectra having integrations of 1.00, 1.45, 1.44, 1.45, and the 40% 4(pyrrol-1-yl)pyridine spectra yielding integrations of 1.00, 1.36, 1.46, 1.46.

The product is yellow in colour and exhibits a band maximum at 463 nm in the UV-visible spectrum, shown in Figure 1. Dilutions of 4(pyrrol-1-yl)pyridine depicted a molar absorptivity of 110 $M^{-1}cm^{-1}$. Solvent dependence was carried out using chloroform, dimethyl sulfoxide, and water; the visible band maxima were recorded at 450 nm, 450 nm, and 463 nm, respectively. These results illustrate a bathochromic shift with increasing solvent polarity, which is typical of a $\pi \rightarrow \pi^*$ transition. However, spin-allowed $\pi \rightarrow \pi^*$ transitions normally yield molar absorptivity values on the order of 10,000-100,000 $M^{-1}cm^{-1}$; thus, the electronic transition observed in this system is highly unusual, *vide infra*.

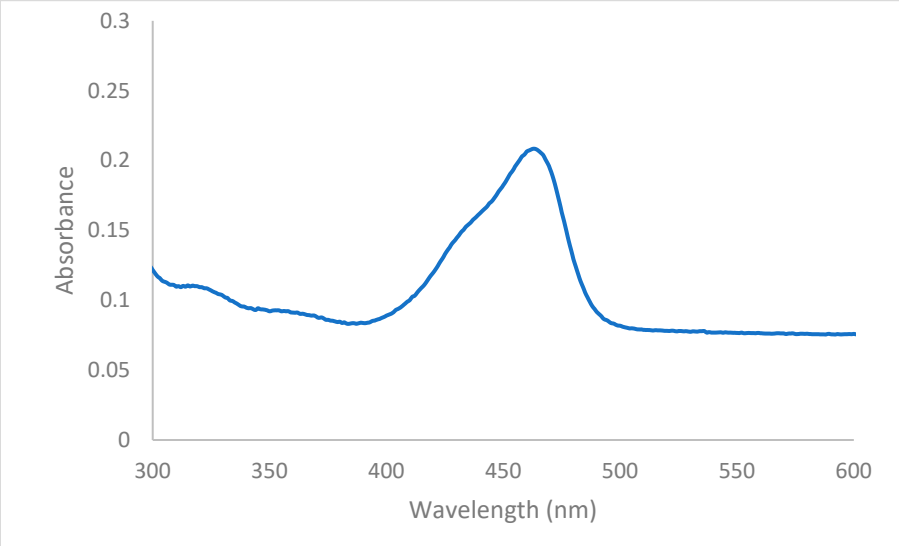

Figure 1. UV-visible spectrum of 4(pyrrol-1-yl)pyridine (2.66 x 10^{-2} M) in 18 MΩ water.

3.2. Anion Sensing by 4(pyrrol-1-yl)pyridine

The compound, 4(pyrrol-1-yl)pyridine, was studied with various anions to determine its anion sensing properties. Upon addition of aqueous sodium nitrite, the system showed a colorimetric change from yellow to pink with increasing absorbance upon each addition of nitrite. Figure 2 illustrates a titration recorded by acquiring UV-visible spectra between the sensor, 4(pyrrol-1-yl)pyridine, and the analyte, $NaNO_2$ (aq). The observed band at 463 nm, indicative of the yellow starting sensor solution, undergoes a bathochromic shift and a new band begins to appear at 509 nm, indicative of the pink final product in solution.

Preprints (www.preprints.org) | NOT PEER-REVIEWED | Posted: 6 December 2023 doi:10.20944/preprints202312.0412.v1

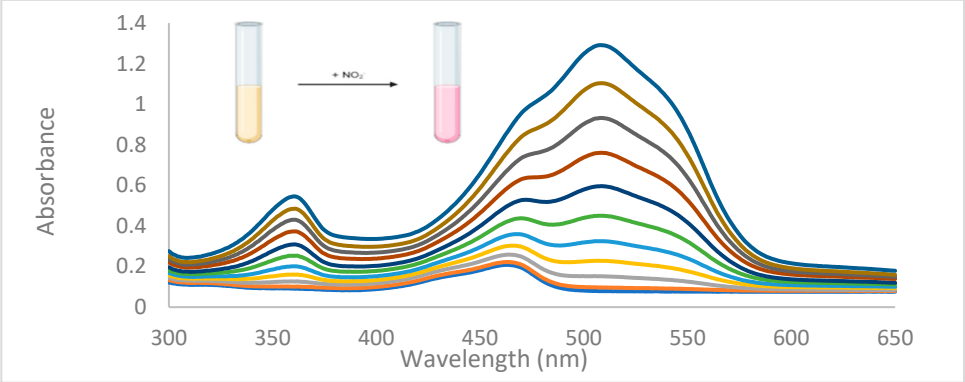

Figure 2. UV-visible spectra of a titration between 4(pyrrol-1-yl)pyridine (1.89 x 10^{-3} M) with increasing 2.00 µL additions of 1.00 x 10^{-2} M sodium nitrite (aq). Initial spectrum is before nitrite addition. Inset illustrates the colorimetric change upon addition of nitrite ion.

Each nitrite addition produced an instantaneous colour change and was found to be irreversible over time. From these results, a limit of detection (LOD) was determined for this sensor system, via a plot of the absorbance changes at 509 nm versus added sodium nitrite concentration, see Figure 3. The LOD was calculated via equation (1), where σ is the standard deviation of the blank and s is the slope of the line generated.

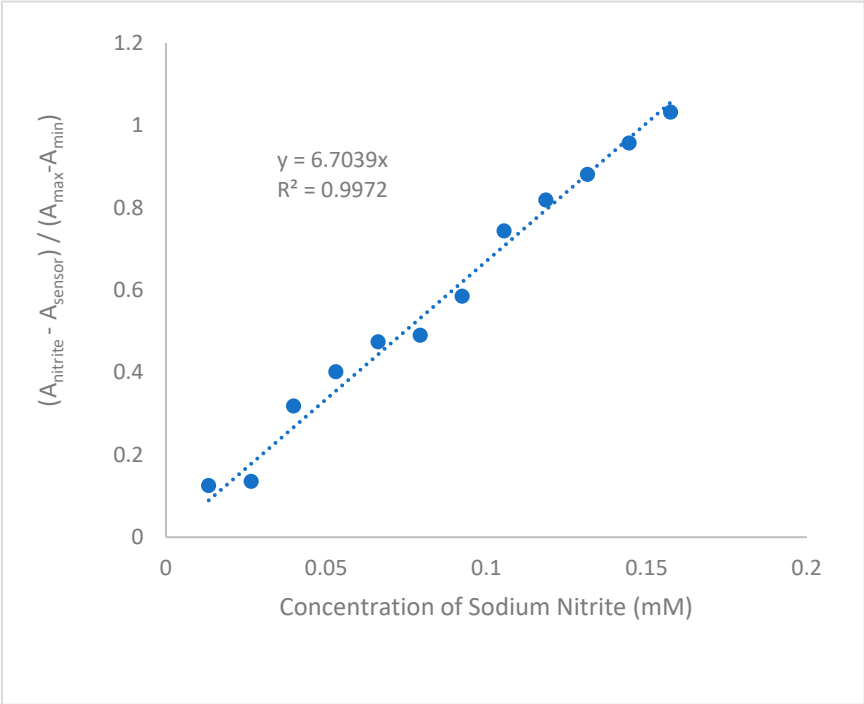

Figure 3. Limit of detection determination of 4(pyrrol-1-yl)pyridine from a plot of absorbance changes at 509 nm on addition of sodium nitrite (aq).

$$LOD = {}^{3\alpha}/_{s} \quad (1)$$

A value of 0.330 (±0.09) ppm was subsequently obtained for these colorimetric changes in 4(pyrrol-1-yl)pyridine upon addition of aqueous sodium nitrite, revealing a high sensitivity of the molecule to added nitrite ion. This result was unaffected by initial sensor concentration.

The selectivity of this system was subsequently investigated using a competitive anion study. Competing anions of SO_3^{2-}, NO_3^-, PO_4^{3-}, SO_4^{-2}, Cl^-, F^-, I^-, Br^-, and CN^- were used in fifty molar equivalents compared to nitrite. After a total of four 1.00 µL additions of each 1:50 aqueous solution,

Preprints (www.preprints.org) | NOT PEER-REVIEWED | Posted: 6 December 2023 doi:10.20944/preprints202312.0412.v1

none displayed any affinity or competitiveness towards 4(pyrrol-1-yl)pyridine. Additionally, in all cases, the colour change to pink upon addition of nitrite was unaffected by the other anion being present and exhibited a minimum percent increase of 62% in the absorbance at 509 nm, see Figure 4. Therefore, the 4(pyrrol-1-yl)pyridine system was found to be both highly sensitive and selective to nitrite ions in aqueous solutions.

3.3. Possible mechanism of sensing

Having established the irreversibility of the colour change, and both the high sensitivity and high selectivity of this system, the mechanism was further investigated. Spectroscopic changes observed in a single injection showed more than a 20% increase of absorbance at 509 nm. The nitrite concentration in solution (1.33×10^{-5} M) is much lower than that of the 4(pyrrol-1-yl)pyridine sensor (2.51×10^{-3} M), illustrating the interaction here is not a simple 1:1 or 1:2 stoichiometry. NMR characterization of the final product proved to be problematic, though. It is common knowledge that pyrroles will react with nitro groups by irreversibly binding at the 2 position on the pyrrole ring [54,56], so this is a hypothesized final product due to the lack of other reagents in solution. However, the system is complicated by what appears to be the formation of an aggregate. As noted above, the visible absorption band at 463 nm with a low molar absorptivity is indicative of $\pi \rightarrow \pi^*$ transitions and π stacking. Moreover, there is a significant absorbance increase at 700 nm, indicative of substantial light scattering, providing further evidence that the product is forming on a supramolecular scale.

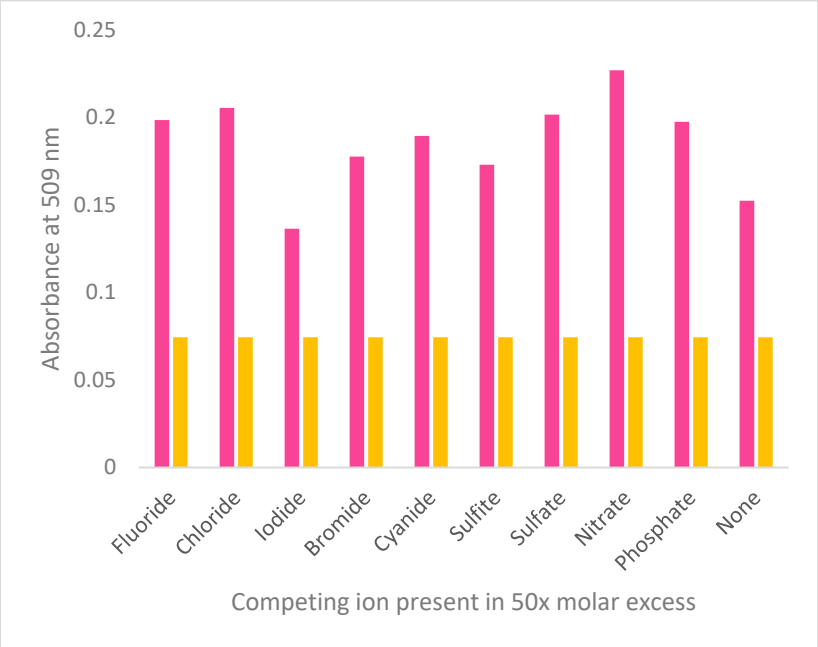

Figure 4. Absorbance at 509 nm of sensor solution (R, purple) and sensor solution with a single 4.00 µL addition of 1.00×10^{-2} M nitrite and 0.5 M competing anion (L, pink).

The presence of an aggregate poses challenges in terms of characterization. It is common for aggregated systems to experience broadening of peaks in NMR analysis due to the many intra-and inter-molecular forces in solution, and even restricted rotation capabilities [57–60]. Previous studies have determined that NMR analysis of molecules dissolved in a liquid crystalline phase is incredibly difficult to decipher due to the large number of spectral transitions present [61].

Raising the concentration of 4(pyrrol-1-yl)pyridine in NMR analysis further broadened the peaks with increasing concentration of the sensor due to the increased presence of aggregates in solution, and the many intermolecular interactions causing the pyridine proton signals to broaden, see Figure 5.

Preprints (www.preprints.org) | NOT PEER-REVIEWED | Posted: 6 December 2023 doi:10.20944/preprints202312.0412.v1

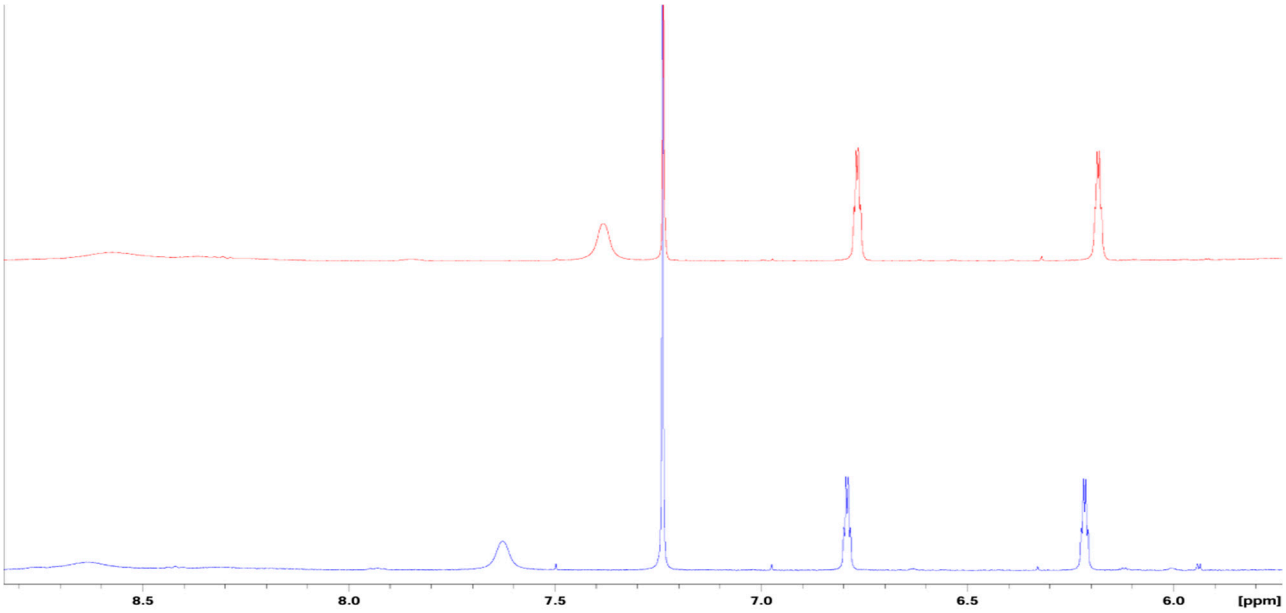

Figure 5. ^{1}H NMR spectra of various concentrations of the oil of 4(pyrrol-1-yl)pyridine in $CDCl_3$. Top to bottom: 40% (v/v), and 10% (v/v).

Typically, highly conjugated systems exhibit broadening in their NMR spectra [62]. The broad components of an NMR spectrum appearing in the aromatic region are due to the formation of π stacking, and arise from the perturbation of shielding effects with subsequent aromatic rings above or below in these supramolecular structures [62]. This is commonly referred to as the "ring current" effect of conjugated aggregate systems. Previous work illustrates this phenomenon with porphyrin systems where ring current effects cause a broadening in the NMR spectrum [63]. Additionally, it has been determined that multiple relaxation mechanisms in ^{1}H NMR can affect line widths, and therefore are more prevalent in spectra of molecules that contain a quadrupolar nucleus, such as a pyridine moiety [61].

In tandem with the line broadening, shifts in location of the aromatic protons are the result of delocalization of electrons from the ring current effect of the π stacking, causing a downfield shift [62]. Hence, the extent of aggregation and overall magnitude of the intermolecular interactions can cause nuclei to have resonances at various shifts [63]. We observed this in the NMR spectrum of the 10% (v/v) sensor solution, where the peaks were shifted downfield, and both signals from the pyridine ring were broadened significantly. Furthermore, the 40% (v/v) sensor solution exhibits an even larger extent of broadening of the pyridine protons.

Consequently, the product with the absorption maximum at 509 nm (sensor-nitrite adduct) would be anticipated to show peak broadening in its NMR. While we were unable to obtain full ^{13}C NMR characterization due to consistently increased baseline noise in the spectrum, we believe the product is a nitro-pyrrole based aggregate with an exceedingly strong electrostatic force between nitrite and the pyrrole end of the 4(pyrrol-1-yl)pyridine system. This would be similar to nitro-pyrrole based moieties that exhibit covalent bond formation at the 2 position on the pyrrole ring [64]. NMR analysis of the final product yields the following shifts in D_2O/H_2O: δ8.65 (d, 2H), δ8.05 (d, 2H), δ6.81 (s, 2H) and δ6.20 (s, 2H) with an approximately 1:10 integration of the pyridine to pyrrole hydrogens, see Supporting Information. Here, the broadening of only the pyrrole peaks from doublets to singlets further supports the increased intermolecular attraction between nitrite and the pyrrole moiety of the 4(pyrrol-1-yl)pyridine system. Additionally, all peaks exhibit a downfield shift due to the intermolecular interaction with nitrite. Two-dimensional COSY NMR revealed that both the pyrrole peaks (δ6.81 and δ6.20) no longer couple with each other. This loss in adjacent proton coupling further corroborates the extreme electrostatic interaction of 4(pyrrol-1-yl)pyridine with nitrite on the pyrrole ring, see Supporting Information.

Preprints (www.preprints.org) | NOT PEER-REVIEWED | Posted: 6 December 2023 doi:10.20944/preprints202312.0412.v1

A quick qualitative test for aggregates in solution is done by employing the Tyndall effect [65–67]. Figure 6 depicts the Tyndall effect in the sensor sample compared to 18 MΩ water. Here, light is scattered if a colloid is present where it is large enough to carry the light through solution; a true solution, like 18 MΩ water, would have no colloids present to scatter the light. Through the use of the Tyndall effect, light was scattered through a solution of 4(pyrrol-1-yl)pyridine confirming the presence of an aggregated species.

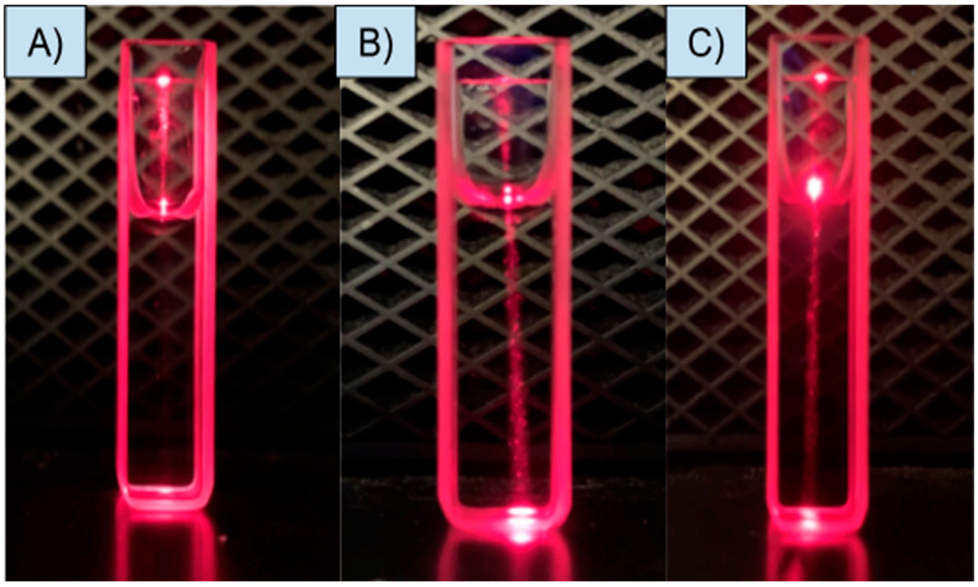

Figure 6. Depiction of the Tyndall effect; (A) 18 MΩ water with no light scattering observable, (B) 4(pyrrol-1-yl)pyridine with light scattering shown, and (C) 4(pyrrol-1-yl)pyridine and nitrite final product with light scattering shown.

To provide an estimate on the extent of aggregation, dynamic light scattering (DLS) is commonly employed to determine a rough estimate of particle size of aggregates or nanoparticles [67,68]. After analysis of aqueous samples of 4(pyrrol-1-yl)pyridine using DLS, an estimate of aggregate size was obtained over a range of concentrations each with five duplicate trials as shown in Table 1. The size was determined using the weighted averages of the DLS values obtained.

Table 1. DLS aggregate size over a range of concentrations of aqueous 4(pyrrol-1-yl)pyridine.

Concentration (M)	Absorbance at 463 nm	Size (nm)
7.20×10^{-3}	0.792	363
6.50×10^{-3}	0.715	249
3.68×10^{-3}	0.405	195
2.11×10^{-3}	0.232	142

Here, it is important to consider that highly aromatic systems have a propensity to aggregate in solution [69–74]. Specifically, conjugated systems, like heterocycles pyridine and pyrrole, have been seen to form aggregates through π-stacking interactions [75–77]. Within this however, different forms can appear with various π-stacking aggregate conformations [77]. It has been reported that when two aromatic moieties absorb in the ultraviolent region of the electromagnetic spectrum, after combining, the newly formed aggregate is likely to absorb in the visible region [77]. This serves to further support an aggregated system between our two aromatic UV absorbing moieties reacting to form a new aggregate absorbing in the visible region (463 nm).

Hunter and Sanders reported four rules with respect to π-stacked aggregates, and that within these stacked systems, they have certain arrangements in their aggregate forms [73]. However, it was discovered that Van Der Waals forces can also contribute to the intensity of the π-stacking, but that they are not controlling the geometry of interaction. Within these structures they stated that, between

Preprints (www.preprints.org) | NOT PEER-REVIEWED | Posted: 6 December 2023 doi:10.20944/preprints202312.0412.v1

two π-interacting systems, stability increases with an electron rich (pyrrole), and electron poor (pyridine) moiety exhibiting π-stacking; here the average pi stacking distance ranges from 3.3-3.8 Å [77]. Therefore, with these rules in mind, the most likely aggregate structures of 4(pyrrol-1-yl)pyridine are shown in Scheme 3.

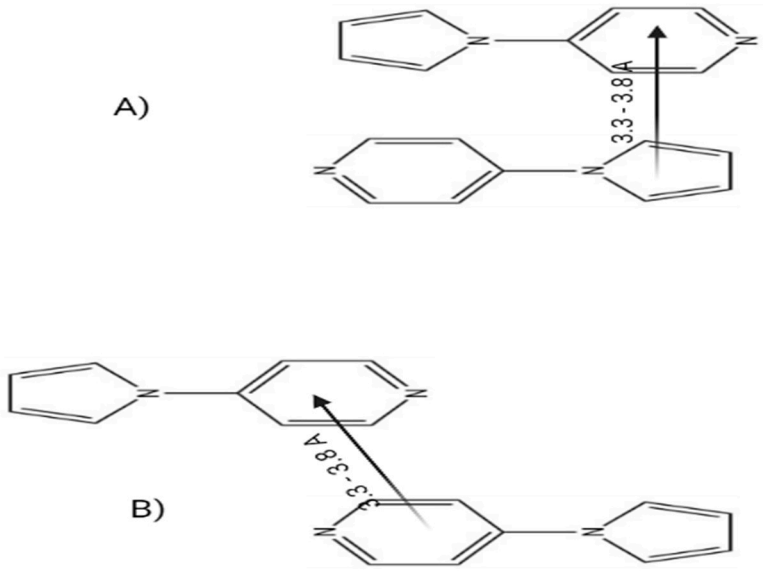

Scheme 3. (A) "face to face" pi stacking of 4(pyrrol-1-yl)pyridine with average pi stacking distance from centroid to centroid from literature values(B) "off-set" pi stacking of 4(pyrrol-1-yl)pyridine with average pi stacking distance from centroid to centroid from literature values.

In further considering the two aggregate structures, "face stacking" has been shown to exhibit hypochromism in solution as opposed to the "off-set" pi stacked system [77]. Knowing this, it is far more likely our 4(pyrrol-1-yl)pyridine system exhibits "off-set" stacking. Further confirmation of an aggregate present is supported by the visible scattering at long wavelengths in the UV-visible spectrum of 4(pyrrol-1-yl)pyridine, and the increased intensity of the nitro-pyrrole based final product absorbance at 509 nm which is highlighted by a deep wine-red hue.

An estimate of approximately 400 to 1,020 monomers for the 4(pyrrol-1-yl)pyridine in solution is reached from the 142-363 nm size range indicated in Table 1 and the mean value of 3.55 Å for the literature value of a centroid to centroid distance of the π-stacked system [74]. Moreover, the previously noted low molar absorptivity value of 110 $M^{-1}cm^{-1}$ is consistent with an intermolecular $\pi \rightarrow \pi^*$ transition in this system.

As previously discussed, ^1H NMR of the 4(pyrrol-1-yl)pyridine system exhibited downfield peak shifting and line broadening. The downfield shifting is indicative of intermolecular interactions in the system. However, the downfield and broadening of only the pyridine protons and not the pyrrole protons further serve to prove the "off-set" stacking of the 4(pyrrol-1-yl)pyridine aggregate. Here, no strong downfield shift or peak broadening would occur with the hydrogens on the pyrrole ring as it is not actively participating in the π-stacking holding the aggregate together.

5. Conclusions

In summary, with the synthesis of 4(pyrrol-1-yl)pyridine we have discovered a new small molecule, colorimetric chemodosimeter for detection of nitrite in aqueous solutions. Simple naked eye detection can be employed with the sensor system experiencing a colour change from yellow to pink, and this reaction is irreversible and instantaneous. The mechanism of sensing is unusual as it involves changes in the degree of aggregation in solution, subsequently affecting the extent of π-stacking, and the intermolecular electronic transitions. This effectively amplifies the nitrite ion

detection, resulting in an extremely low limit of detection of 0.330 (±0.09) ppm, and meeting the criteria for the maximum contaminate levels from both the WHO and EPA. Overall, the sensor system may prove to be valuable for nitrite detection in the food industry as it possesses several important features such as low cost, rapid testing, ease of analysis, high sensitivity, and high selectivity.

Supplementary Materials: The following supporting information can be downloaded at the website of this paper posted on Preprints.org. Figure S1: ^{1}H NMR of dilute (<10% v/v) 4(pyrrol-1-yl)pyridine in CDCl3 with integrations; Figure S2: ^{13}C NMR of 4(pyrrol-1-yl)pyridine in CDCl3 with peak locations from NMR solvent; Figure S3: DEPT 90 ^{13}C NMR of 4(pyrrol-1-yl)pyridine in $CDCl_3$. Peak observed at 53.85 ppm is indicative of residual dichloromethane following extraction. Quaternary carbons do not appear in the spectrum.; Figure S4: HSQC NMR of dilute (<10% v/v) 4(pyrrol-1-yl)pyridine in CDCl3. Peak observed at 5.2 ppm is indicative of residual dichloromethane following extraction.; Figure S5: COSY NMR of dilute (<10% v/v) 4(pyrrol-1-yl)pyridine in CDCl3. Peak observed at 5.2 ppm is indicative of residual dichloromethane following extraction; Figure S6: ^{1}H NMR of 10% (v/v) 4(pyrrol-1-yl)pyridine in CDCl3. Solvent peak observed at 7.24ppm., Figure S7: ^{1}H NMR of 40% (v/v) 4(pyrrol-1-yl)pyridine in CDCl3. Solvent peak observed at 7.24ppm.; Figure S8: ^{1}H NMR of dilute 4(pyrrol-1-yl)pyridine and nitrite final product in D_2O/H_2O . Solvent peak observed at 4.80 ppm.; Figure S9: COSY NMR for dilute 4(pyrrol-1-yl)pyridine and nitrite final product in D_2O/H_2O. Solvent peak appearing at 4.80 ppm..

Author Contributions: M.E.T conducted all the experimental work. All participated in the development of design and methodology. All performed data analysis. A.J.L. supervised the research project. M.E.T and A.J.L wrote the article, and all approved the final version of the manuscript.

Funding: Funding was obtained from the Department of Chemistry, and the office of Entrepreneurship and Innovation Partnerships at Binghamton University.

Institutional Review Board Statement: Not applicable.

Informed Consent Statement: Not applicable.

Data Availability Statement: No data were used for this research article.

Acknowledgments: We thank Binghamton University faculty, Professors Susan Bane, Chuan-Jian Zhong, and Hiuyuan Guo for access to instrumentation and Dr. Juergen Schulte for his valuable NMR expertise.

Conflicts of Interest: The authors declare no conflict of interest. The funders had no role in the design of the study; in the collection, analyses, or interpretation of data; in the writing of the manuscript; or in the decision to publish the results.

References

1. United States Environmental Protection Agency. *National Primary Drinking Water Regulations: Contaminant Specific Fact Sheets*, Inorganic Chemicals, consumer version; Washington DC, 1995.
2. Moorcroft, M.J.; Davis, J.; Compton, R.G. *Talanta*, 2001, **54**, 785-803.
3. Fanning, J.C. *Coord. Chem. Rev.* 2000, **199**, 159-179.
4. Nollet, L.M.L.Handbook of Water Analysis, 2000.
5. Guidelines for drinking water quality, 2nd ed. Addendum to Vol. 2. Health criteria and other supporting information. World Health Organization, Geneva, 1998.
6. Rajasulochana, P.; Ganesan, Y.; Kumar, P.S.; Mahalazmi, S.; Tasneem, F.; Ponnuchamy, M.; Kapoor, A. Paper-Based Microfluidic Colorimetric Sensor on a 3D Printed Support for Quantitative Detection of Nitrite in Aquatic Environments. *Environmental Research*, 2022, **208**, 112745.
7. Burt, T.P.; Howden, N.J.K.; Worral, F.; Whelan, M.J. Long-term monitoring of river water nitrate: how much data do we need? *J. Environ. Monit.* 2010, **12**, 71-79.
8. Carpenter, S.R.; Caraco, N.F.; Correll, D.L.; Howarth, R.W.; Sharpley, A.N.; Smit, V.H. Nonpoint pollution of surface waters with phosphorus and nitrogen. *Ecol. Appl.* 1998, **8**. 559-568.
9. Cameron, K.C.; Di, H.J.; Moir, J.L. Nitrogen losses from the soil/plant system: a review. *Ann. Appl. Biol.* 2013, **162**, 145-173.
10. Zia, H.; Harris, N.R.; Merrett, G.V.; Rivers, M.; Coles, N. The impact of agricultural activities on water quality: A case for collaborative catchment-scale management using integrated wireless sensor networks. *Comput. Electron. Agr.* 2013, **96**, 126-138.

11. Ahmad, R.; Ahn, M.S.; Hahn, Y.B. A highly sensitive nonenzymatic sensor based on Fe_2O_3 nanoparticle coated ZnO nanorods for electrochemical detection of nitrite. *Adv. Mater. Interfaces,* 2017, **4**, 1700691-1700700.
12. Li, X.R.; Kong, F.Y.; Liu, J; Liang, T.M; Xu, J.J; Chen, H.Y. Synthesis of Potassium-Modified Graphene and its Application in Nitrite-Selective Sensing. *Adv. Funct. Mater.* 2012, **22**, 1981-1988.
13. Ye.D.; Luo, L.; Chen, Q.; Liu, X. A novel nitrite sensor based on graphene/polypyrrole/chitosan nanocomposite modified glassy carbon electrode. *Analyst.* 2011, **136**, 4563-4569.
14. Zuane, J.D. Handbook of Drinking Water Quality, 2nd ed.; 1996.
15. Zhang, L.; Huang, J.; Hu, Z.; Li, X.; Ding, T.; Hou, X.; Chen, Z.; Ye, Z.; Luo, R. $Ni(NO_3)^{2-}$ induced high electrocatalytic hydrogen evolution performance of self-supported fold like WC coating on carbon fiber paper prepared through molten salt method, *Electrochem. Acta.* 2022, **422**, 140553.
16. Zhe, T.; Li, R.; Li, F.; Liang, S.; Shi, D.; Sun, X.; Liu, Y.; Cao, Y.; Bu, T,; Want, L. Surface Engineering of Carbon Selenide Nanofilms on Carbon Cloth: An Advanced and Ultrasensitive Self- Supporting Binder-Free Electrode for Nitrite Sensing. *Food Chem.* 2021, **340**, 127953.
17. Sihto, H.M.; Budi Susila, Y.; Tasara, T.; Radstrom, P.; Stephan, R.; Schelin, J.; Johler, S. Effect of Sodium Nitrite and Regulatory Mutations ΔagrA, ΔsarA, and ΔsigB on the MRNA and Protein Levels of Staphylococcal Enteroxtoxin. *D. Food Control.* 2016, **65**, 37-45.
18. Akyuz, M.; Ata, S. Determination of Low-Level Nitrite and Nitrate in Biological, Food, and Environmental Samples by Gas Chromatography-Mass spectrometry and Liquid Chromatography with Fluorescence Detection. *Talanta.* 2009, **79**, 900-904.
19. Hospital, X.F.; Hierro, E.; Arnau, J.; Carballo, J.; Aguirre, J.S.; Gratacos-Cubarsi, M.; Fernandex, M. Effect of Nitrate and Nitrite on Listeria and Selected Spoilage Bacteria Inoculated in Dry-Cured Ham. *Food. Res. Int.* 2017, **101**, 82-87.
20. Abdulmumeen, H.A.; Risikat, A.N.; Sururah, A.R. Food: its preservatives, additives, and applications. *Int. J. Chem. Biochem. Sci.* 2012, **1**, 36-47.
21. Chen, X.; Chen, X, Zhu, L.; Liu, W.; Jiang, L. Programming an orthogonal self-assembling protein cascade based on reactive peptide-protein pairs for in vitro enzymatic trehalose production. *J. Agric. Food. Chem.* 2022, **70**, 4690-4700.
22. Larson, S.C.; Bergkvist, L.; Wolk, A. Processed Meat Consumption, Dietary Nitrosamines and Stomach Cancer Risk in a Cohort of Swedish Women. *Int. J. Cancer.* 2006, **119**, 915-919.
23. Neth, M.R.; Love, J.S.; Horowitz, B.Z.; Shertz, M.D.; Sahni, R.; Daya, M.R. Fatal sodium nitrite poisoning: key considerations for prehospital providers. *Prehosp. Emerg. Care.* 2021, **25**, 844-850.
24. Manassaram, D.M.; Backer, L.C.; Moll, D.M. A Review of Nitrates in Drinking Water: Maternal Exposure and Adverse Reproductive and Developmental Outcomes. *Environ. Health Perspect.* 2006, **114**, 320-324.
25. Bryan. N.S.; Fernandez, B.O.; Bauer, S.M.; Garcia-Saura, M.F.; Milson, A.B.; Rassaf, T.; Maloney, R.E.; Bharti, A.; Rodriguez, J.; Feelisch, M. Nitrite is a Signalling Molecule and Regulator of Gener Expression in Mammalian Tissues. *Nat. Chem. Biol.* 2005, **1**, 290-297.
26. Ye, D.; Luo, L.; Ding, Y.; Chen, Q.; Liu, X. Synthesis of Potassium-Modified Graphene and its Application in Nitrite-Selective Sensing. *Analyst.* 2011, **136**, 4563-4569.
27. Song, P.; Wu, L.; Guan, W. Dietary nitrates, nitrites, and nitrosamines intake and the risk of gastric cancer: a meta-analysis. *Nutrients.* 2015, **7**, 9872-9895.
28. Balimandawa, M.; de Meester, C.; Leonard, A. The mutagenicity of nitrite in the Salmonella/microsome test system. *Mutat. Res., Genet. Toxicol.* 1994, **321**, 7-11.
29. Ma, L.; Hu, L.; Feng, X.; Wang, S. Nitrate and Nitrite in Health and Disease. *Aging Dis.* 2018, **9**, 938-945.
30. Shepard, S.E. Endogenous formation of N-nitroso compounds in relation to the intake of nitrate or nitrite. In: Health aspects of nitrate and its metabolites. 1995, 137-150.
31. Fan, A.M.; Steinberg, V.E. Health implications of nitrate and nitrite in drinking water: an update on methemoglobinemia occurrence and reproductive and developmental toxicity. *Regul Toxicol. Pharmacol.* 1996, 35-43.
32. Puangpila, C.; Jakmunee, J.; Pencharee, S.; Pensrisirikul, W. Mobile-phone based colorimetric analysis for determining nitrite content in water. *Environ. Chem.* 2018, **15**, 403-410.
33. Ward, M.H.; Mark, S.D.; Cantor, K.P.; Weisenburger, D.D.; Correa-Villasenor, A.; Zahm, S.H. Drinking Water Nitrate and the Risk of Non-Hodgkin's Lymphoma. *Epidemiology.* 1996, **7**, 465-471.

34. World Health Organization. Nitrate and Nitrite in Drinking Water Background Document for Development of Drink Water. 2009, **2**, 21.
35. Bagheri, H.; Hajian, A.; Rezaei, M.; Shirzadmehr, A. Composite of Cu metal nanoparticles-multiwall carbon nanotubes-reduced graphene oxide as a novel and high-performance platform of the electrochemical sensor for simultaneous determination of nitrite and nitrate. *J. Hazard. Mater.* 2017, **324**, 762-772.
36. Li, Y.; Zhang, X.; Sun, Y.; Yang, Z.; Liu, J. Fabrication Non-Enzymatic Electrochemical Sensor Based on Methyl Red and Graphene Oxide Nanocomposite Modified Carbon Paste Electrode for Determination of Nitrite in Food Samples. *Int. J. Electrochem. Sci.* 2023, **18**, 100097.
37. Nussler, A.K.; Glanemann, M.; Schirmeier, A.; Liu, L.; Nussler, N.C. Fluorometric measurement of nitrite/nitrate by 2,3-diaminonaphthalene. *Nat. Protoc.* 2006, **1**, 2223-2226.
38. Ohta, T.; Arai, Y.; Takitani, S. Fluorometric determination of nitrite with 4-hydroxycoumarin. *Anal. Chem.* 1986, **58**, 3132-3135.
39. Adarsh, N.; Shanmugasundaram, M.; Ramaiah, D. Efficient Reaction Based Colorimetric Probe for Sensitive Detection, Quantification, and on-Site Analysis of Nitrite Ions in Natural Water Resources. *Anal. Chem.* 2013, **85**, 10008-10012.
40. Singh, L.; Ranjan, N. Highly Selective and Sensitive Detection of Nitrite Ion by an Unusual Nitration of a Fluorescent Benzimidazole. *J. Am. Chem. Soc.* 2023, **145**, 2745-2749.
41. Shou, Y.; Yan, D; Wei, M.; A 2D quantum-dot based electrochemiluminescence film sensor towards reversible temperature-sensitive response and nitrite detection. *J. Mater. Chem.* 2015, **3**, 10099-10106.
42. Garside, C. A chemiluminescent technique for the determination of nanomolar concentrations of nitrate and nitrite in seawater. *Mar. Chem.* 1982, **11**, 159-167.
43. Chen, H.; Fang, Y.; An, T.; Zhu, K.; Lu, J. Simultaneous spectrophotometric determination of nitrite and nitrate in water samples by flow-injection analysis. *Int. J. Environ. Anal. Chem.* 2000, **76**, 89-98.
44. European Standard. Water quality-determination of nitrites-molecular absorption spectrometric method. 1993.
45. Fox, J.B. *J. Anal. Biochem.* 1979, **51**, 1493.
46. Guembe-Garcia, M.; Gonzalez-Ceballos, L.; Arnaiz, A.; Fernandez-Muino, M.A.; Sancho, M.T.; Oses, S.M.; Ibeas, S.; Rovira, J.; Melero, B.; Represa, C.; Garcia, J.M.; Vallejos, S. Easy Nitrite Analysis of Processed Meat with Colorimetric Polymer Sensors and a Smartphone App. *ACS Appl. Matter. Interfaces.* 2022, **14**, 37051-37058.
47. Zhao, W.; Yang, H.; Xu, S.; Li, X.; Wei, W.; Liu, X. "Olive-Structured" Nanocomposite Based on Environmental Nitrite Detection. *ACS Sustain. Chem. Eng.* 2019, **7**, 17424-17431.
48. Lin, B.; Xu, J.; Lin, K.; Li, M.; Lu, M. Low-Cost Automatic Sensor for In Situ Colorimetric Detection of Phosphate and Nitrite in Agricultural Water. *ACS Sens.* 2018, **3**, 2541-2549.
49. Gu, Z.; Wu, M.L.; Yan, B.Y.; Wang, H.F.; Kong, C. Integrated Digital Microfluidic Platform for Colorimetric Sensing of Nitrite. *ACS Omega.* 2020, **5**, 11196-11201.
50. Seki, K.; Ohkura, K.; Terashima, N.; Kanaoka, Y. Photoreaction of 4-iodopyridine with Herteroaromatics. *Heterocycles.* 1986, **24**, 799.
51. Barckholtz, C.; Barckholz, T.A.; Hadad, C.M. C-H and N-H Bond Dissociation Energies of Small Aromatic Hydrocarbons. *J. Am. Chem. Soc.* 1999, **121**, 491-500.
52. Schmitt, L.; Lees, A.J.; US 2020/0363382. 2020.
53. Chen, H.; Wang, Q.; Tao, F.; A Novel Palladium-catalyzed Amination of aryl Halides with Amines using rac-P-Phos as the Ligand. *Chinese Journal of Chemistry,* 2009, **27,** 1382-1386.
54. Pai, G.; Asoke, P.C. Ligan-free Copper Nanoparticle promoted N-arylation of azoles with aryl and heteroaryl iodides, *Tetrahedron Letters.* 2014, **55,** 941-944.
55. Teo, Y.C.; Yong, F.F.; Sim,S. Ligand-free Cu_2O-catalyzed cross coupling of nitrogen heterocycles with iodopyridines. *Tetrahedron,* 2013, **69,** 7279-7284.
56. Ding, X.B.; Brimble, M.A.; Furkert, D.P. Reactivity of 2-Nitropyrrole Systems: Development of Improved Synthetic Approaches to Nitropyrrole Natural Products. *J. Org. Chem.* 2018, **83**, 12460-12470.
57. Morgan, K.J.; Morrey, D.P. Nitropyrroles-I. *Tetrahedron.* 1966, **22**, 57-62.
58. Hills, B.P.; Takacs, S.F.; Belton, P.S. The Effects of Proteins on the Proton N.M.R. Transverse Relaxation Time of Water. *Molec. Phys.* 1989, **67**, 919-937.
59. McGarrity, J.F.; Ogle, C.A. High-Field Proton NMR Study of the Aggregation and Complexation of N-Butyllithium in Tetrahydrofuran. *J. Am. Chem. Soc.* 1985, **107**, 1805-1810.

60. Okazawa, N.; Sorensen, T.S. The Line-Shape Analysis of Nuclear Magnetic Resonance Peaks Broadened by the Presence of a "hidden" Exchange Partner. *Canadian Journal of Chemistry.* 1978, **56**, 2737-2742.
61. Imbardelli, D.; Chidichiomo, G.; Longeri, M. Nuclear Relaxation of Partially Oriented Pyridine Determined by Line Width Analysis of ^{1}H NMR Spectra. *Chem. Phys. Lett.* 1987, **135**, 319-324.
62. Parteni, F.; Tassinari, F.; Libertini, E.; Lanzi, M.; Mucci, A. π-Stacking Signature in NMR Solution Spectra of Thiophene-Based Conjugated Polymers. *ACS Omega.* 2017, **2**, 5775-5784.
63. Gjuroski, I.; Furrer, J.; Vermathen, M. Probing the Interactions of Porphyrins with Macromolecules using NMR Spectroscopy Techniques. *Molec.* 2021, **26**, 1942-1985.
64. Becker, E.; Bradley, R. Effects of "Ring Currents" on the NMR Spectra of Porphyrins. *J. Chem. Phys.* 1959, **31**, 1413-1414.
65. Jerlov, N.G.; Kullenber, B. The Tyndall Effect of Uniform Minerogenic Suspensions. *Tellus.* 1953, **5**, 306-307.
66. Xiao, W.; Deng, Z.; Huang, Z.; Zhuang, M.; Yuan, Y.; Nie, J.; Zhang, Y. Highly Sensitive Colorimetric Detection of a Variety of Analytes via the Tyndall Effect. *Anal. Chem.* 2019, **91**, 15114-15122.
67. Bender, M. The Use of Light Scattering for Determining Particle Size and Molecular Weight and Shape. *J. Chem. Educ.* 1952, **29**, 15.
68. Kanjanawarut, R.; Yuan, B.; Xiano, D.S. UV-Vis Spectroscopy and Dynamic Light Scattering Study of Gold Nanorods Aggregation. *Nucleic Acid Therapeutics.* 2013, **23**, 273-280.
69. Duff, D.G.; Kirkwood, D.J.; Stevenson, D.M. The Behaviour of Dyes in Aqueous Solutions. I. The Influence of Chemical Structure on Dye Aggregation a Polarographic Study. *J. Soc. Dyes. Colour.* 1977, **93**, 303-306.
70. Navarro, A.; Sanz. F. Dye aggregation in solution: Study of C.I. direct red I. *Dyes. Pigments.* 1999, **40**, 131-139
71. Martinez-Manez, R.; Sancenon, F. Fluorogenic and Chromogenic Chemosensors, and Reagents for Anions. *Chem. Rev.* 2003, **103,** 4419-4476.
72. Yu, H.: Aziz, H. Direct Observation of Exciton-Induced Molecular Aggregation in Organic Small-Molecule Electroluminescent Materials. *J. Phys. Chem. C.* 2019, **123**, 16424-16429.
73. Gao, M.; Tang, B.Z. Fluorescent Sensors Based on Aggregation-Induced Emission: Recent Advances and Perspectives. *ACS Sens.* 2017, **2**, 1382-1399.
74. Graham, D.J. Information Content in Organic Molecules: Aggregation States and Solvent Effects. *J. Chem. Inf. Model.* 2005, **45**, 1223-1236.
75. Martinez, C.R.; Iverson, B.L. Rethinking the Term "Pi-Stacking". *Chem. Sci.* 2012, **3**, 2191.
76. Hunter, C.A.; Sanders, J.K. The Nature of Pi-Pi Interactions. *J. Am. Chem. Soc.* 1990, **112**, 5525-5534.
77. Janiak, C. A Critical Account on π-π Stacking in Metal Complexes with Aromatic Nitrogen-Containing Ligands. *J. Chem. Soc.* 2000, **21**, 3885-3896.